



Si-decorated photoanodes for dye sensitised solar cells

E.V. Tekshina^{a,*}, A.S. Steparuk^b, R.A. Irgashev^b, V.Y. Nesterov^c, D.V. Shuleiko^c,
M.A. Teplonogova^a, D.A. Krupanova^d, V.V. Emets^e, V.N. Andreev^e, V.A. Grinberg^e,
S.A. Kozyukhin^a

^a Kurnakov Institute of General and Inorganic Chemistry of the Russian Academy of Sciences, Moscow, 119991, Russia

^b Postovsky Institute of Organic Synthesis, Ural Branch of the Russian Academy of Sciences, Ekaterinburg, 620137, Russia

^c Lomonosov Moscow State University, Moscow, 119991, Russia

^d Moscow Institute of Physics and Technology (National Research University), Moscow, 141701, Russia

^e Frumkin Institute of Physical Chemistry and Electrochemistry of the Russian Academy of Sciences, Moscow, 119071, Russia

ARTICLE INFO

Keywords:

Silicon
Nanoparticles
Dye-sensitized solar cells
Surface modification
Photovoltaic efficiency

ABSTRACT

In this work, modification of nanocrystalline TiO₂ photoanodes consisting of 20 nm diameter spheres for dye-sensitized solar cells (DSSCs), by introducing silicon nanoparticles (Si-NPs) of different sizes, larger than TiO₂ particles, obtained by two different pulsed laser technologies: mesoporous silicon ablation and micron-sized silicon powder fragmentation was studied. The distribution of various types of particles in the functional layer of the photoanode was obtained using scanning electron microscopy and energy-dispersive X-ray analysis. The effect of Si-NP size on photovoltaic properties was demonstrated. Dye-sensitized photoanodes modified with mezo Si-NPs demonstrated 17 % increase in short-circuit current (j_{sc}) and increased energy conversion efficiency due to reduced electron recombination and improved charge collection compared to unmodified TiO₂. Thus, the obtained results on modification of the surface of TiO₂ photoanodes with Si-NPs have potential for improving the efficiency and stability of DSSCs.

1. Introduction

Dye-sensitized solar cells (DSSCs), a subject of investigation spanning over three decades since their inception in 1991, epitomize a distinct category of cost-effective photovoltaic devices [1–3]. Characterized by a straightforward fabrication process devoid of intricate vacuum apparatus requirements, DSSCs offer an economically viable avenue for production. The accessibility of functional materials theoretical efficiency limit of $\eta = 33\%$ has garnered significant interest among researchers. Unlike conventional solar cells reliant on p-n junction principles, where semiconductor materials serve as the light-absorbing layer and photogenerated carrier separation transpires at the semiconductor interface, DSSC architecture delineates distinct roles for charge carrier generation, separation, and transport across different functional materials [4–6]. This compartmentalization presents a compelling prospect from a materials science perspective, allowing researchers to concentrate efforts on enhancing the functional properties of individual components without perturbing others, thereby observing resultant impacts on overall device efficiency.

The operational mechanism of DSSCs revolves around the absorption of light by a dye (commonly referred to as a sensitizer) adsorbed

onto a semiconductor layer, initiating the photoexcitation of an electron within the dye molecule, which is subsequently injected into the conduction band of nanocrystalline TiO₂. Subsequent reduction of the dye species takes place via processes facilitated within the liquid mediator system, typically an electrolyte, where electrons are transferred from the cathode. Thus, the DSSC operates as a closed cyclic system sustained by a fraction of the photogenerated electrons.

A diverse array of dyes finds application in dye-sensitized solar cells (DSSCs), encompassing compounds sourced from natural origins to intricately structured complexes featuring a variety of metals, often characterized by elevated atomic numbers [7–9]. Among these, Ru(II) complexes stand out as particularly efficacious, currently achieving efficiencies of 11.9 % for individual cells and 10.4 % for minimodules [10]. However, the synthesis of such dyes entails complexity, necessitates expensive precursors, and consequently, engenders a high production cost. Notwithstanding these challenges, notable advancements have been realized in the realm of metal-free (organic) dyes. These alternatives offer the advantages of comparatively straightforward synthesis, employing more readily available starting materials, rendering them economically appealing despite their marginally diminished efficiency compared to ruthenium-based counterparts.

* Corresponding author.

E-mail address: ekaterina3141@mail.ru (E.V. Tekshina).

<https://doi.org/10.1016/j.tsf.2025.140652>

Received 7 September 2024; Received in revised form 2 February 2025; Accepted 7 March 2025
0040-6090/© 20XX

The analysis presented above underscores a substantial dissonance between the theoretically predicted efficiency and the realized performance in practical applications, largely attributable to the prevalence of "parasitic" reactions—commonly referred to as back reactions—in DSSCs, alongside a constellation of unresolved challenges pertaining to functional materials [11–13]. Nonetheless, notwithstanding these obstacles, DSSC technology remains widely regarded by experts as the preeminent solution currently available for a spectrum of specialized applications. These applications capitalize on the unique amalgamation of properties offered by DSSCs, including their cost-effectiveness, non-toxicity, visually appealing color palette, transparency, and exceptional performance under low-light and ambient illumination conditions [14].

Currently, a relevant direction is the modification of components in DSSC to enhance their efficiency. Research is being conducted to improve each element of the cell, particularly the modification of the semiconductor layer, which includes enhancing its optical and electrical properties. This investigation focuses on the modification of nanocrystalline TiO₂, comprising spheres approximately 20 nm in diameter and serving as the photoanode, through the incorporation of larger silicon nanoparticles (Si-NPs) derived from two distinct methodologies, both involving the utilization of pulsed laser techniques for silicon ablation or defragmentation. The impetus for this research stems from previously obtained theoretical and experimental findings suggesting that augmenting nanocrystalline titanium oxide layers with submicron particles enhances solar cell efficiency. Notably, A. Usami's Monte Carlo simulations [15] demonstrated that elongating the photon absorption pathway within nanocrystalline films, coupled with optical confinement achieved through total internal reflection from surfaces, markedly enhances light absorption in sensitized films. Furthermore, it was elucidated that the enhancement in efficiency attributed to optical confinement outweighs that resulting from increased absorption pathway length. Subsequent experimental validations corroborated these findings, coining the observed phenomenon as the "haze concept" [16]. It was discerned that the efficiency of solar-to-electric energy conversion escalates with heightened "haze" of the electrode. However, a drawback of this method lies in the propensity for larger nanoparticles to diminish the specific surface area of the semiconductor layer, thereby impacting the dye filling degree. Noteworthy investigations [16,17] have underscored that silicon-modified TiO₂ exhibits enhanced stability and diminished charge recombination, further influencing DSSC efficiency. In aggregate, the modification of mesoporous TiO₂ with Si-NPs emerges as a promising avenue for enhancing the efficiency and stability of DSSCs.

The nanoparticles incorporated into photoanodes to enhance their light trapping efficiency can be either plasmonic nanoparticles of noble metals [18,19] or semiconductor nanoparticles [16,17]. However, application of Au or Ag for such photoanodes can increase their cost. Additionally, incorporation of metallic nanoparticles can lead to short-circuiting of the solar cell due to the formation of filaments from

nanoparticles with metallic conductivity when the percolation threshold in the photoanode is locally exceeded. Therefore, incorporation of semiconductor nanoparticles into the photoanodes seems more promising. Among semiconductors silicon is a widespread and accessible material, which can be converted into nanoparticles by a variety of methods [20], including colloidal synthesis [21], mechanical grinding, and the liquid-phase laser synthesis [22]. In our work we chose the latter approach for Si-NPs production. Implemented in the one-stage method of pulsed laser ablation in liquid, it provides nanoparticle's formation without undesirable chemical impurities compared to wet chemistry methods [23–25]. It also allows obtaining nanoparticles in a wide range of sizes [22,23,26,27]. We should note that the mechanical grinding method for obtaining particles with a size small enough for successful incorporation into photoanodes requires additional chemical treatment of the material before grinding, for example, fabrication of porous silicon membranes from crystalline silicon wafers [28], or alternatively, it can be used as a first stage for subsequent fragmentation of nanoparticles by laser radiation [29].

Consequently, in our research, we focused on the ramifications of modifying nanocrystalline TiO₂ with Si-NPs of various sizes on the performance of solar cells. The investigation aimed to outline the effects of introducing 10–100 nanometer- or submicron-scaled particles into a nanocrystalline titanium oxide layer, particularly focusing on light absorption processes, optical confinement, and the overall efficiency of sensitized films. Addressing this objective entails identifying the optimal conditions for modification to attain maximal efficiency when integrating organic dyes into TiO₂-based solar cell configurations.

2. Experimental details

2.1. Fabrication of silicon nanoparticles

We used two different ways to make Si-NPs (Fig. 1). The first approach involved ablating targets composed of mesoporous silicon through laser irradiation featuring picosecond pulse duration. These targets were fabricated from mesoporous silicon obtained via electrochemical etching techniques. Boron-doped Si *p*+ -type wafers with a surface crystallographic orientation of (100) and a resistivity of 10–20 mΩ·cm served as the initial substrates. The etching process utilized a solution comprising 47.5 % hydrofluoric acid (HF) mixed with ethanol (C₂H₅OH) in a 1:1 ratio. Before etching, the silicon wafer substrates were briefly immersed in pure hydrofluoric acid to remove the natural oxide layer from the surface. The etching current density was maintained at 20 mA/cm², with an etching duration of 40 min. Fabrication of silicon nanoparticle suspensions involved irradiating the prepared targets in a cell containing distilled water by picosecond laser pulses (Nd:YAG laser EKSPLA PL 2143A, λ=1064 nm, pulse duration τ=34 ps, pulse repetition frequency *f* = 10 Hz, pulse energy *E* = 10 mJ) over a period of 20 min. The water layer above the target had a

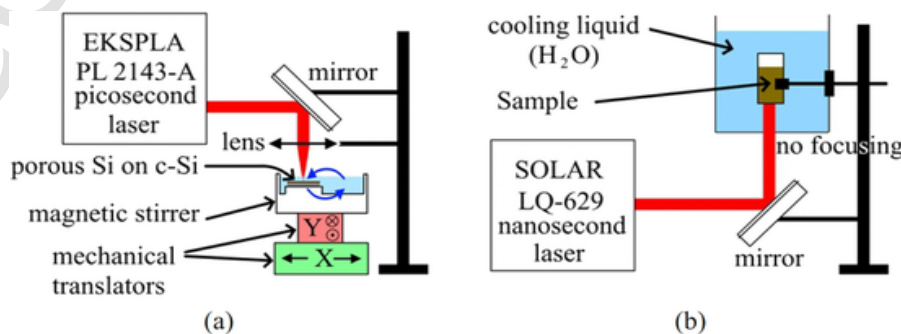


Fig. 1. Schemes of the setups used to make (a) mezo Si-NPs and (b) sub-micro Si-NPs.

thickness of approximately ~ 2 mm, and mixing within the cell was facilitated using a magnetic stirrer to achieve homogeneity in the suspension. Samples prepared by this method were labeled as mezo.

The second method aimed to produce submicron-sized Si-NPs via fragmentation using nanosecond laser pulses on silicon powder consisting of particles with ~ 5 μm average size, preliminarily obtained through mechanical milling. The powder was placed in a glass cylindrical container with a volume of 3 mL at a concentration of 5 mg/mL in distilled water, followed by irradiation with laser pulses for 7 min. A nanosecond Solar LQ-629 laser was employed, operating at $\lambda = 1064$ nm, $\tau = 12$ ns, $f = 100$ Hz, and $E = 200$ mJ. Laser irradiation was directed perpendicular to the bottom of the container without focusing, with the laser beam diameter on the container's bottom measuring 5 mm. To maintain cooling during irradiation, the container with the suspension was submerged in water. Subsequently, the container with the irradiated suspension was allowed to settle for approximately ~ 30 min to allow large, unfragmented particles to settle to the bottom, after which the remaining suspension containing fragmented submicron particles was transferred to another container. Samples prepared by this method were labeled as sub-micro.

2.2. Fabrication of unmodified and Si-NPs-modified TiO₂ photoanodes sensitized with the dye

The study employed commercially available photoanodes featuring mesoporous TiO₂ layers, Solaronix. The active area is 0.36 cm² and layer thickness is 10–15 μm . Colloidal solutions of Si-NPs were deposited onto the active region of the photoanodes using a volume of 50 μL . The mass content of silicon nanoparticles in 50 μL of suspension is 25 μg , which corresponds to 10^{11} particles in the case of mesoparticles (average diameter 75 nm) and 10^8 particles for submicron suspensions (average diameter 600 nm). Following application, the samples were air-dried at room temperature and then subjected to annealing at 300 °C for 1 hour to ensure thorough removal of water from the pores. This is the temperature at which no changes occur in the structure or composition of either titanium dioxide or Si-NPs [30,31]. The sensitization of modified photoanodes was carried out using the organic dye IS 4, which we previously investigated in [32,33]; the molecular structure of the dye is depicted in Fig. 2. As a reference sample, a photoanode sensitized with the dye IS 4 without Si-NPs deposit was used. Sensitization was achieved by immersing the photoanodes in chloroform dye solution with a concentration of $C = 5 \cdot 10^{-4}$ mol/L, followed by a 24-hour exposition in solution at room temperature, after which the photoanodes were air-dried.

2.3. Characterizations

For photo-electrochemical measurements a three-electrode cell PECC-2 (Zahner Elektrik) was used. The TiO₂ photoanode (0.36 cm²) with adsorbed dyes served as the working electrode and a platinum wire with the surface area of 5 cm² was used as the auxiliary electrode. A silver wire was the quasi-reference electrode. The redox electrolyte comprised a mixture of 0.5 M LiI + 0.05 M I₂ in acetonitrile. Voltam-

metric measurements were performed using an IPC Pro MF potentiostat. The working electrode was illuminated by a Newport 96,000AM 1.5 solar spectrum simulator with an intensity of 100 mW/cm², and the illumination power was monitored with a Nova apparatus (OPHIR-SPIRICON Inc.). To further investigate the photoelectrochemical properties of the dye-sensitized photoanode incident photon-to-current conversion efficiency (IPCE), intensity modulated photocurrent spectroscopy (IMPS), intensity modulated photovoltage spectroscopy (IMVS) measurements were conducted [34,35]. IPCE, IMPS and IMVS measurements were conducted on a ZAHNER's CIMPS-QE/IPCE workstation, with the working electrode illuminated by a tunable light-source (TLS03). IMVS were taken without superposition of external polarization, i.e., under open circuit (OC) conditions. IMPS were recorded under short-circuit (SC) conditions.

Phase analysis of the samples was performed using X-ray powder diffraction (XRD) with a Bruker D8 Advance powder X-ray diffractometer (Cu K α radiation) in the angular range of 10° - 70° with a step size of 0.02° 2 θ and a dwell time of at least 0.4 s per step. The identification of the diffractograms was carried out using the ICDD PDF2 database (2012). The Raman scattering spectra were obtained using the SOL Instruments Confotec NR500 confocal Raman spectrometer. The spectral range for Raman signal registration spans from 30 cm⁻¹ to 2000 cm⁻¹. A diode-pumped solid-state laser operating at 532 nm with a power of 25–50 mW was utilized for the measurements. The optical microscope was equipped with a 20x objective lens (NA = 0.50), enabling detailed observation of the samples. The spectral resolution achieved during the measurements was 0.25 cm⁻¹. This setup allows for high-precision, non-destructive analysis of the physical and chemical properties of micro-objects and nanostructures through optical spectroscopy methods. The surface morphology of the obtained photoanodes and the elemental composition of the titanium dioxide functional layer were investigated using Scanning electron microscopy (SEM) and Energy dispersive X-ray spectroscopy (EDS) methods. SEM images were taken using a Tescan Amber GMH scanning electron microscope. Images were obtained using an Everhart-Thornley SE detector at $\times 3.000$ – 100.000 magnifications and at an accelerating voltage of 1 kV. EDS spectra and EDS elemental maps were recorded using an Ultim MAX EDS detector with a 100 mm² active area (Oxford Instruments) and at an accelerating voltage of 20 kV using AZtec 5.0 SP1 software.

3. Results and discussion

Fig. 3 shows the results of photovoltaic investigations for the fabricated photoanodes: (a) current-voltage characteristics (J/V curves); (b) incident photon-to-current conversion efficiency (IPCE); (c) intensity modulated photovoltage spectroscopy and (d) intensity modulated photocurrent spectroscopy. The photovoltaic results are summarized in Table 1.

The average efficiency values along with confidence interval errors for 3 parallel devices

It is riveting to notice the open-circuit voltage (V_{oc}) remains unchanged during modification and amounts to $V_{oc} = 0.69$ V, while the short-circuit current (J_{sc}) increases by approximately 17 % in the case of the photoanode modified with Si-NPs (mezo), which in turn reflects in the enhancement of the power conversion efficiency (PCE), despite a slight reduction in the fill factor (FF).

As seen in Fig. 3b, the IPCE spectra of photoanodes increases after their modification, particularly noticeable for titanium dioxide modified with Si-NPs (mezo). This result correlates with the results shown in Fig. 3a. Therefore, it can be hypothesized that the enhancement in the efficiency of the photoanodes is partly attributed to the increased quantum yield within the spectral range corresponding to the peak of the solar spectrum.

From the IMVS and IMPS spectra (on Fig. 3c and 3d) the values of the electron transfer time (τ_{tr}), electron lifetime (τ_{rec}), charge collection

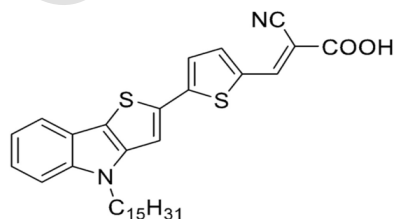


Fig. 2. Molecular structure of IS 4 dye.

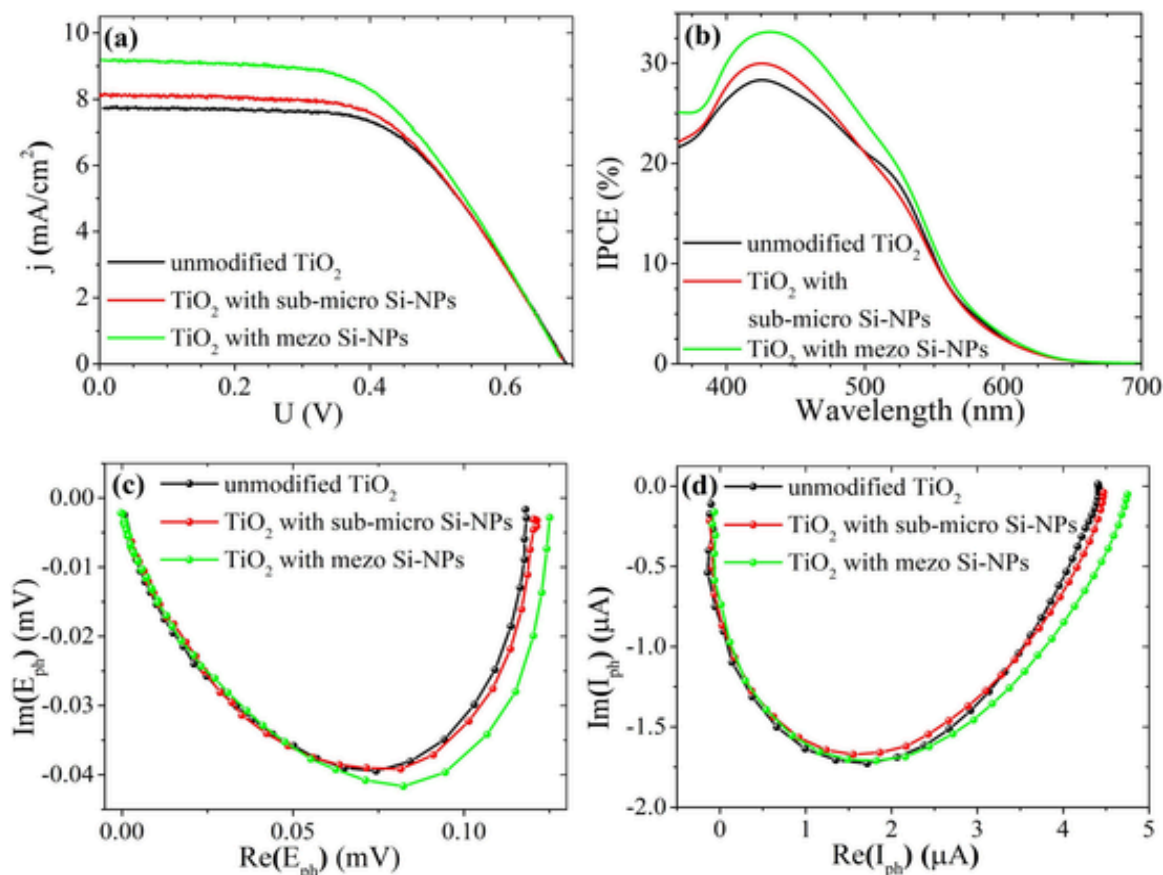


Fig. 3. (a) J/V curves, (b) IPCE spectra, (c) IMVS and (d) IMPS spectra for unmodified and Si-NPs modified TiO₂ photoanodes sensitized with the dye IS 4.

Table 1
Photovoltaic performance of photoanodes.

Photoanode	V_{oc} (V)	j_{sc} (mA/cm ²)	FF (%)	PCE (%)
unmodified TiO ₂	0.69 ± 0.01	7.80 ± 0.06	56.50 ± 2.00	3.00 ± 0.05
modified TiO ₂ with sub-micro Si-NPs	0.69 ± 0.01	8.10 ± 0.07	56.50 ± 2.00	3.15 ± 0.03
modified TiO ₂ with mezo Si-NPs	0.69 ± 0.01	9.15 ± 0.07	53.50 ± 1.60	3.40 ± 0.03

efficiency (η_{cc}), electron diffusion coefficient (D_e) and effective electron diffusion length (L_d) were obtained, which are summarized in Table 2.

The photoanodes modified with Si-NPs based on nanocrystalline TiO₂ have a reduced transit time (τ_{tr}) by approximately 20 %, a higher electron diffusion coefficient, and consequently a greater diffusion length of photocarriers, which results in higher conductivity. The IS 4 mezo photoanode also exhibits an increased electron lifetime due to reduced charge recombination and improved charge collection efficiency. Thus, the modified TiO₂ demonstrates an enhanced electron diffusion coefficient and electron lifetime, which reduces recombination losses and contributes to increased PCE.

It can be seen that the efficiency of a photoanode depends on several factors, among which the ability of the material to absorb photons upon irradiation and generate electrons capable of reaching the external electrode without recombining is crucial. The aforementioned experimental results demonstrate that modifying titanium dioxide using Si-NPs is a promising approach for the discussed photovoltaic devices and could be applied in practical activities. To gain a deeper understanding of the physicochemical nature of the influence of Si-NPs on titanium dioxide,

Table 2

Electron transfer time (τ_{tr}), lifetime of excited electron (τ_{rec}), charge collection efficiency (η_{cc}), active layer thickness (D_e), and effective electron diffusion time (L_d) obtained from the IMPS and IMVS spectra of the photoanodes tested.

Photoanode	τ_{tr} (ms)	τ_{rec} (ms)	η_{cc}	$D_e \cdot 10^{-3}$ (cm ² ·s ⁻¹)	L_d (μm)
unmodified TiO ₂	0.51	14.50	0.96	1.90	52
modified TiO ₂ with sub-micro Si-NPs	0.40	14.50	0.97	2.40	59
modified TiO ₂ with mezo Si-NPs	0.40	17.60	0.98	2.40	65

The electron transfer time (τ_{tr}) was estimated from the IMPS spectra using the equation: $\tau_{tr} = \frac{1}{2\pi f_{tr}}$;

The electron lifetime (τ_{rec}) was estimated from the IMVS spectra using the equation: $\tau_{rec} = \frac{1}{2\pi f_{rec}}$;

The charge collection efficiency (η_{cc}) was determined by the equation: $\eta_{cc} = 1 - \frac{\tau_{tr}}{\tau_{rec}}$;

The electron diffusion coefficient (D_e) was calculated using the equation: where L is the thickness of the electrode ($\sim 15 \mu\text{m}$): $D_e = \frac{L^2}{2.35 \cdot \tau_{tr}}$;

The effective electron diffusion length (L_d) was determined by the equation: $L_d = \sqrt{D_e \cdot \tau_{rec}}$.

we conducted additional studies on both the initial Si-NPs colloidal solutions and the titanium dioxide after modification.

It is important to note that, contrary to the studies suggesting the haze effect in photoanodes, the enhancement of efficiency through the incorporation of silicon nanoparticles is not attributed to optical

changes but rather to functional improvements. Specifically, the presence of semiconductor nanoparticles enhances charge carrier transport within the functional layer and increases electron diffusion length by decorating defects. Additionally, contrary to expectations, we do not observe an increase in the dye filling factor; rather, it decreases. This may be related to the fact that the nanoparticles themselves occupy the pores, leaving less space for the integration of dye molecules.

The sizes of the Si-NPs were determined using SEM. For this purpose, drops of Si-NPs suspensions were deposited on silicon substrates and evaporated. The diameters of the nanoparticles were measured, and histograms of the size distributions of the formed Si-NPs were constructed. The sample size for the histograms was 250 particles for the mezo sample and 410 particles for the micro sample. The results are presented in Fig. 4.

To investigate the surface composition of the photoanodes before and after modification, we obtained X-ray diffraction patterns of the surfaces and recorded Raman scattering spectra, as shown in Fig. 5a and 5b, respectively.

The registered diffraction reflections can be clearly attributed to the characteristic maxima of anatase TiO_2 (JCPDS-ICDD: 21-1272). The diffraction peaks of anatase TiO_2 at approximately 25.3; 37.8; 38.5; 48.0; 53.9; 55.1; 61.5; 62.8, and 65.6 correspond to the orientations (101), (004), (112), (200), (105), (211), (203), (204), and (116), respectively. The peak around 26.5 corresponds to the rutile phase with the orientation (110). Based on the X-ray diffraction data after modifi-

cation, we observed the same pattern, and the particles could not be detected.

According to the provided data [36,37], the anatase phase of TiO_2 predominantly exhibits a characteristic line consisting of six main modes, which include A_{1g} (519 cm^{-1}), B_{1g} (399 cm^{-1} and 519 cm^{-1}), and E_g (144 cm^{-1} , 197 cm^{-1} , and 639 cm^{-1}). The spectra for all investigated samples with silicon particles, including the unmodified sample, showed peaks of active modes at 144 cm^{-1} , 197 cm^{-1} , 397 cm^{-1} , 518 cm^{-1} , and 639 cm^{-1} . This directly confirms the presence of the pure anatase phase, the absence of other rutile phase peaks, and no peaks characteristic of silicon nanoparticles [38]. This result may indicate that there are no particles on the surface or that their quantity is insufficient for us to observe a response from them. The particles did not anchor to the surface, and if any remained, they are likely those that ended up inside the cracks or pores of the mesoporous layer film.

The surface morphology of the modified photoanodes and the elemental composition of the titanium dioxide functional layer are shown in Figs. 6-9.

As can be seen from the SEM data obtained using the secondary electron signal, there are large spherical particles on the surface of nanocrystalline titanium dioxide. The size of these particles is approximately equal to that of the silicon particles in the coarse fraction shown in Fig. 6a and ranges from about 400 to 700 nm.

The distribution of Si-NPs over the surface is uniform, but the conglomerations of several nanoparticles are mainly observed. After exam-

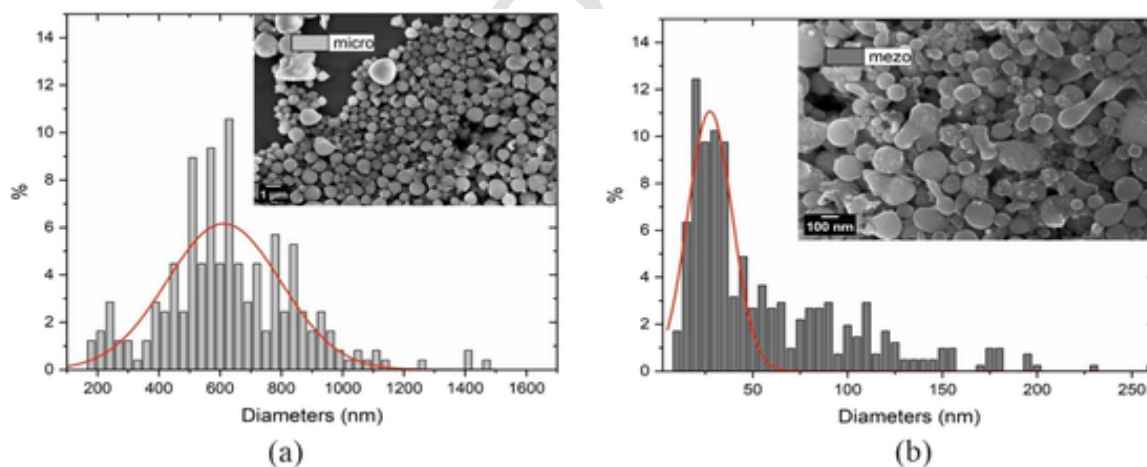


Fig. 4. Particle size distribution histograms: (a) Si-NPs (sub-micro); (b) Si-NPs (mezo).

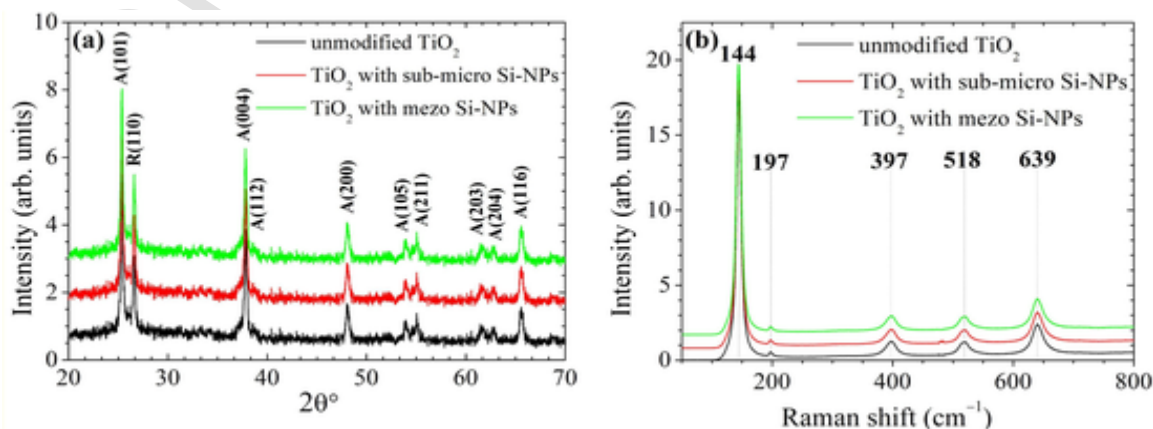


Fig. 5. (a) X-ray diffraction patterns of the surfaces, (b) Raman scattering spectra.

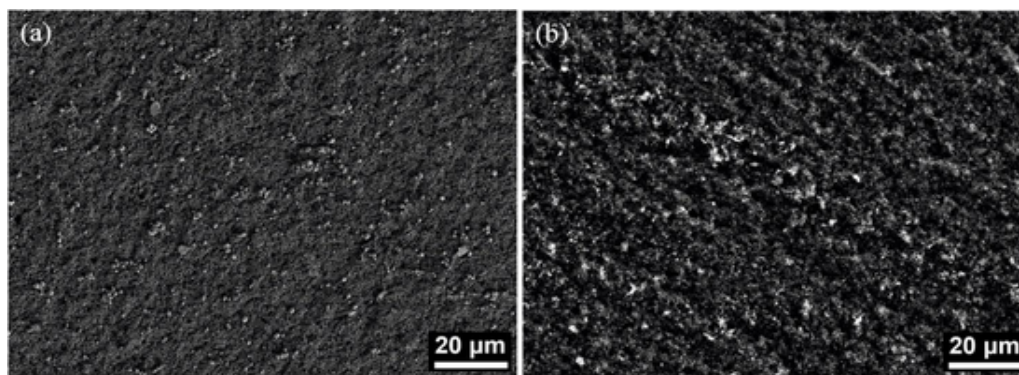


Fig. 6. SEM Images of the titanium dioxide surface modified with Si-NPs (sub-micro), obtained using SEM: (a) immediately after nanoparticle deposition; (b) after optical studies.

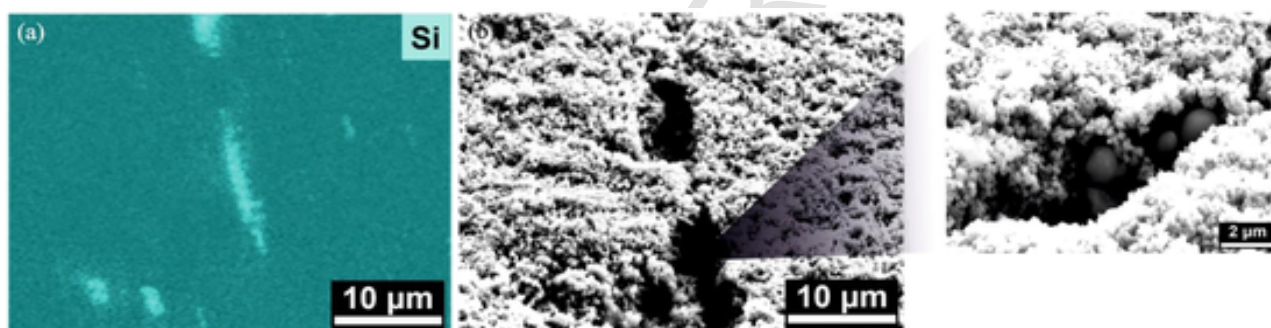


Fig. 7. Appearance of Si nanoparticles in the cracks of the mesoporous TiO_2 layer: (a) EDS map to (b) SEM image compared. The inset shows SEM image of Si-NPs within the crack.

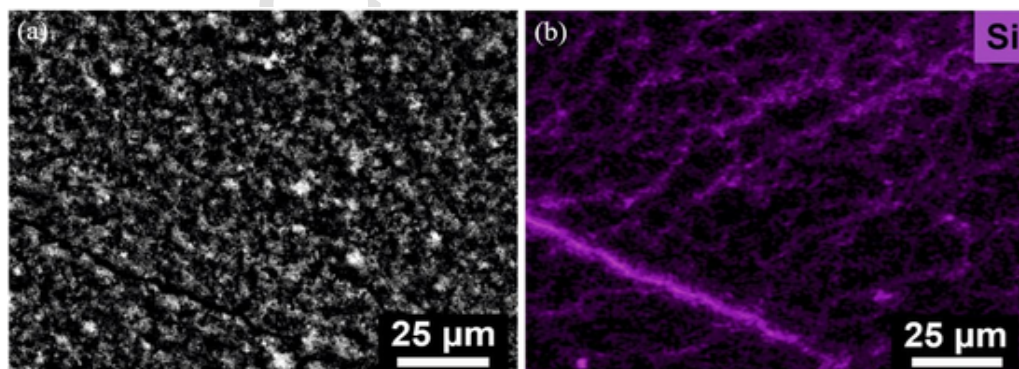


Fig. 8. (a) Microphotograph of the surface of a mesoporous TiO_2 layer modified with Si-NPs (mezo), and (b) an EDS map showing the Si concentration on the same surface and in the cracks of the mesoporous TiO_2 layer.

ination, no particles were found on the surface (Fig. 6b), which indicates that there is no chemical bond between the silicon particles and the surface of the porous layer of titanium dioxide, and the particles are attached to the surface only due to physical bonds, roughness, or surface defects. To illustrate, in Fig. 7a, we see silicon nanoparticles that have become trapped in a crack in the film.

To figure out the presence of Si-NPs in the samples after optical measurements, the EDS elemental mapping was performed. The obtained EDS map shown in Fig. 7b also indicates Si-NPs hidden in cracks and pores of TiO_2 surface.

Thus, it was confirmed that the particles we see in the cracks are indeed silicon. However, we do not observe 200 nm-sized and smaller particles in SEM images. One assumption is that small silicon nanoparticles have penetrated into the pores of nanocrystalline titanium dioxide to a depth greater than the thickness of the surface layers from which secondary electrons and characteristic X-ray radiation were detected.

To verify this statement and determine the nature of the distribution of 200 nm-size and smaller Si-NPs on the surface of the photoanode, SEM images were taken and EDS maps were recorded for the photoanode modified with 10–200 nm silicon NPs (mezo), see Fig. 9a and b.

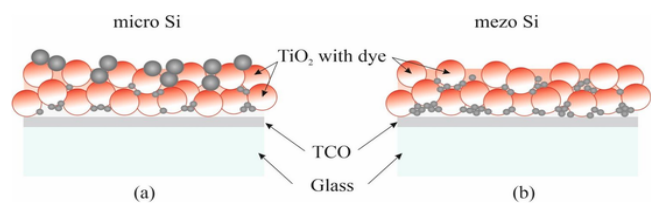


Fig. 9. Scheme of Si-NPs distribution in the photoanode. a — sub-micro. b — mezo.

Fig. 8a shows the surface of a layer of titanium dioxide without large particles on it. However, in Fig. 8b, there is a clear signal from silicon particles that have penetrated into a crack and remained on the surface due to the developed relief of the titanium dioxide layer.

Thus, it can be assumed that the silicon particles have integrated into the photoanode according to the scheme shown in Fig. 9.

As shown in Fig. 9, the distribution of silicon particles within the porous TiO_2 film varies depending on their size. Si-NPs (sub-micro), measuring several hundred nanometers, attach only to the rough surface and large cracks of the functional layer, with a small fraction of smaller particles, sized below 100–200 nanometers, penetrating deeper into the pores. In the case of mezo particles, predominantly sized in the several tens of nanometers range, the Si-NPs fill smaller pores and cracks in the titanium dioxide layer, penetrating deep into it. These Si-NPs (mezo) are better retained within the photoanode, compared to the sub-micro particles, resulting in the formation of a silicon interlayer located closer to the conductive glass and the decoration of defects in the porous functional layer. However, the incorporation of Si-NPs (sub-micro) is also quite promising, as the limited contribution to efficiency improvement may be due to the particles not being well anchored in the semiconductor layer of the photoanode. Therefore, we believe that this issue warrants separate attention in future research. One approach to improve the nanoparticles retention in the photoanode could be fabrication of nanoparticle ensembles with a smaller average size and its standard deviation, which, when using pulsed laser ablation, could be achieved, for example, by changing the buffer medium [22]. Another approach could be, in contrast, increasing the size and/or number of pores in the photoanode. However, the size and concentration of the pores should not be high, as this will reduce the filling factor in the photoanode and, accordingly, reduce its efficiency. Thus, an alternative approach could be to functionalize the surface of the nanoparticles as well as the surface of the photoanode before the nanoparticle's deposition. It is also worth considering a combination of nanoparticles of different types – both semiconductor nanoparticles in the bulk of the photoanode and metallic nanoparticles on the surface – to combine the effect of increased conductivity, the haze effect and plasmonic resonances [18].

4. Conclusion

Thus, the modification of titanium dioxide with silicon nanoparticles was demonstrated to be a promising approach for the efficiency improvement of photovoltaic devices.

Despite Si-NPs being removed from the surface of the photoanode during measurements, a sufficient amount of them was entrenched in cracks and pores of the TiO_2 surface. These silicon nanoparticles embedded into the TiO_2 relief were still able to increase the efficiency of the photoanode. It can be concluded that the inclusion of large silicon particles on the surface contributes to an increase in efficiency to a lesser extent, since they cannot be sufficiently effectively attached. The introduction of nanoparticles, contrary to expectations, does not increase the FF. In the case of submicron particles, it even reduces this parameter. This phenomenon is attributed to the fact that the nanoparticles occupy the pores, thereby leaving less space for the integration of

dye molecules. The main influence on improving the performance of solar cells is exerted precisely by particles with sizes of about 100 nm, which fill the cracks in the functional layer of the photoanode. Such so-called photoanode decoration by Si-NPs leads to PCE enhancement as well as short-circuit current increase up to 17 % in the dye-sensitized nanocrystalline TiO_2 photoanodes.

To achieve the effect on the photoanodes by modifying them with nanoparticles, it is necessary to achieve reliable incorporation of these nanoparticles into the photoanode matrix or reliable retention of them on the surface. When using nanoparticles as-prepared by pulsed laser ablation, only small-sized particles (200 nm and smaller) can be embedded into the bulk of the photoanode or retained in cracks on its surface. Thus, only the effect from the incorporation of small nanoparticles is observed, manifesting itself in increasing the conductivity of photoanodes. On the other hand, observation of the "haze concept" from larger nanoparticles is limited by the necessity to improve their retention inside the photoanode or on its surface.

All results are surprising yet valuable. Considering the challenges associated with the integration of larger particles, future work can focus on refining the technology for their incorporation. This will allow us to address existing shortcomings and potentially lead to a more significant enhancement in the efficiency of the devices. This can be achieved either by changing the photoanode porosity parameters or by functionalization of the nanoparticle surface to improve their adhesion to the photoanode surface.

CRediT authorship contribution statement

E.V. Tekshina: Writing – original draft, Visualization, Methodology, Investigation. A.S. Steparuk: Investigation. R.A. Irgashev: Investigation. V.Y. Nesterov: Investigation. D.V. Shuleiko: Investigation. M.A. Teplonogova: Investigation. D.A. Krupanova: Visualization, Investigation. V.V. Emets: Methodology, Investigation. V.N. Andreev: Investigation. V.A. Grinberg: Investigation. S.A. Kozyukhin: Supervision, Conceptualization, Project administration, Methodology.

Declaration of competing interest

The authors declare that they have no known competing financial interests or personal relationships that could have appeared to influence the work reported in this paper.

Acknowledgements

This work was supported by the Ministry of Science and Higher Education of the Russian Federation as part of the State Assignment of the Kurnakov Institute of General and Inorganic Chemistry (1022060900147-6-1.4.2) and Frumkin Institute of Physical Chemistry and Electrochemistry of the Russian Academy of Sciences. The synthesis of compound IS 4 was carried out with the financial support from the Ministry of Education and Science of the Russian Federation within the framework of the state assignment (subject no state. reg. 124020100137-7). The analysis of the composition and structure of the materials obtained was carried out using the equipment of the JRC PMR IGIC RAS.

Data availability

Data will be made available on request.

References

- [1] B. O'Regan, M. Grätzel, A low-cost, high-efficiency solar cell based on dye-sensitized colloidal TiO_2 films, *Nature* 353 (1991) 737–740, <https://doi.org/10.1038/353737a0>.
- [2] M. Grätzel, Solar energy conversion by dye-sensitized photovoltaic cells, *Inorg. Chem.* 44 (20) (2005) 6841–6851, <https://doi.org/10.1021/ic0508371>.

- [3] S. Bai, A.K. Amiruddin, A.K. Pandey, M. Samykano, M.S. Ahmad, K. Sharma, V.V. Tyagi, Advancements in the development of various types of dye-sensitized solar cells: a comparative review, *Energy Eng. J. Assoc. Energy Eng.* 118 (4) (2021) 737–759, <https://doi.org/10.32604/EE.2021.016157>.
- [4] B.A. Gregg, Excitonic solar cells, *J. Phys. Chem. B* 107 (2003) 4688–4698, <https://doi.org/10.1021/jp022507x>.
- [5] L. Jin, J. Zhai, L. Heng, T. Wei, L. Wen, L. Jiang, X. Zhang, Bio-inspired multi-scale structures in dye-sensitized solar cells, *J. Photochem. Photobiol. C* 10 (2009) 149–158, <https://doi.org/10.1016/j.jphotochemrev.2009.10.002>.
- [6] S. Tontapha, P. Uppachai, V. Amornkitbamrung, Fabrication of functional materials for dye-sensitized solar cells, *Frontiers Energy Res.* 9 (2021) 641983, <https://doi.org/10.3389/fenrg.2021.641983>.
- [7] Y. Kusumawati, A.S. Hutama, D.V. Wellia, R. Subagyo, Natural resources for dye-sensitized solar cells, *Heliyon* 7 (12) (2021), <https://doi.org/10.1016/j.heliyon.2021.e08436>.
- [8] S.V. Tatarin, E.A. Meshcheriakova, S.A. Kozyukhin, V.V. Emets, S.I. Bezzubov, Rational design of efficient photosensitizers based on cyclometalated iridium (III) complexes with 2-arylbenzimidazole and aromatic 1, 3-diketone ligands, *Dalton Trans.* 52 (44) (2023) 16261–16275, <https://doi.org/10.1039/D3DT02789A>.
- [9] G. Richhariya, A. Kumar, P. Tekasakul, B. Gupta, Natural dyes for dye sensitized solar cell: a review, *Renew. Sustain. Energy Rev.* 69 (2017) 705–718, <https://doi.org/10.1016/j.rser.2016.11.198>.
- [10] M.A. Green, E.D. Dunlop, M. Yoshita, N. Kopidakis, K. Bothe, G. Siefert, X. Hao, Solar cell efficiency tables (version 62), *Prog. Photovoltaics Res. Appl.* 31 (7) (2023) 651–663, <https://doi.org/10.1002/ppp.3726>.
- [11] J. Villanueva-Cab, H. Wang, G. Oskam, L.M. Peter, Electron diffusion and back reaction in dye-sensitized solar cells: the effect of nonlinear recombination kinetics, *J. Phys. Chem. Lett.* 1 (4) (2010) 748–751, <https://doi.org/10.1021/jz1000243>.
- [12] P.J. Cameron, L.M. Peter, How does back-reaction at the conducting glass substrate influence the dynamic photovoltage response of nanocrystalline dye-sensitized solar cells, *J. Phys. Chem. B* 109 (15) (2005) 7392–7398, <https://doi.org/10.1021/jp0407270>.
- [13] A. Sen, M.H. Putra, A.K. Biswas, A.K. Behera, A. Groß, Insight on the choice of sensitizers/dyes for dye sensitized solar cells: a review, *Dyes Pigm.* 213 (2023) 111087, <https://doi.org/10.1016/j.dyepig.2023.111087>.
- [14] A.B. Muñoz-García, I. Benesperi, G. Boschloo, J.J. Concepcion, J.H. Delcamp, E.A. Gibson, G.J. Meyer, M. Pavone, H. Pettersson, A. Hagfeldt, M. Freitag, Dye-sensitized solar cells strike back, *Chem. Soc. Rev.* 50 (22) (2021) 12450–12550, <https://doi.org/10.1039/D0CS01336F>.
- [15] A. Usami, Theoretical simulations of optical confinement in dye-sensitized nanocrystalline solar cells, *Solar Energy Mater. Solar Cells.* 64 (2000) 73–83, [https://doi.org/10.1016/S0927-0248\(00\)00049-0](https://doi.org/10.1016/S0927-0248(00)00049-0).
- [16] Y. Chiba, A. Islam, Y. Watanabe, R. Komiya, N. Koide, L. Han, Dye-sensitized solar cells with conversion efficiency of 11.1%, *Jpn. J. Appl. Phys.* 45 (7L) (2006) L638, <https://doi.org/10.1143/JJAP.45.L638>.
- [17] X.Z. Guo, W.Z. Shen, Optimization of the scattering design in photoelectrode for dye-sensitized solar cells by theoretical simulation, *J. Appl. Phys.* 114 (2013), <https://doi.org/10.1063/1.4818438>.
- [18] M. Ghidelli, L. Mascaretti, B.R. Bricchi, A. Brognara, T.A. Afifi, V. Russo, C.S. Casari, A.L. Bassi, Light management in TiO₂ thin films integrated with Au plasmonic nanoparticles, *Semicond. Sci. Technol.* 35 (3) (2020) 035016, <https://doi.org/10.1088/1361-6641/ab6cea>.
- [19] G. Qin, A. Watanabe, Formation of textured microstructure by mist deposition of TiO₂ nanoparticles, *J. Nanopart. Res.* 15 (2013) 1–11, <https://doi.org/10.1007/s11051-013-2084-5>.
- [20] H. Sugimoto, M. Fujii, Colloidal Mie resonant silicon nanoparticles, *Nanotechnology* 32 (45) (2021) 452001, <https://doi.org/10.1088/1361-6528/ac1a44>.
- [21] A. Shavel, L. Guerrini, R.A. Alvarez-Puebla, Colloidal synthesis of silicon nanoparticles in molten salts, *Nanoscale* 9 (24) (2017) 8157–8163, <https://doi.org/10.1039/c7nr01839h>.
- [22] O.I. Eroshova, P.A. Perminov, S.V. Zaboltnov, M.B. Gongal'skii, A.A. Ezhov, L.A. Golovan', P.K. Kashkarov, Structural properties of silicon nanoparticles formed by pulsed laser ablation in liquid media, *Crystallogr. Rep.* 57 (2012) 831–835, <https://doi.org/10.1134/S1063774512030066>.
- [23] R. Intartaglia, K. Bagga, M. Scotto, A. Diaspro, F. Brandi, Luminescent silicon nanoparticles prepared by ultra short pulsed laser ablation in liquid for imaging applications, *Opt. Mater. Express.* 2 (5) (2012) 510–518, <https://doi.org/10.1364/OME.2.000510>.
- [24] N.G. Semaltianos, G. Karczewski, Laser synthesis of magnetic nanoparticles in liquids and application in the fabrication of polymer–nanoparticle composites, *ACS Appl. Nano Mater.* 4 (7) (2021) 6407–6440, <https://doi.org/10.1021/acsnam.1c00715>.
- [25] R. Intartaglia, K. Bagga, F. Brandi, G. Das, A. Genovese, E. Di Fabrizio, A. Diaspro, Optical properties of femtosecond laser-synthesized silicon nanoparticles in deionized water, *J. Phys. Chem. C* 115 (12) (2011) 5102–5107, <https://doi.org/10.1021/jp109351t>.
- [26] S. Yang, W. Cai, H. Zhang, X. Xu, H. Zeng, Size and structure control of Si nanoparticles by laser ablation in different liquid media and further centrifugation classification, *J. Phys. Chem. C* 113 (44) (2009) 19091–19095, <https://doi.org/10.1021/jp907285f>.
- [27] I.O. Dzhun, V.Y. Nesterov, D.V. Shuleiko, S.V. Zaboltnov, D.E. Presnov, Y.A. Alekhina, E.A. Konstantinova, N.S. Perov, N.G. Chechenin, Magnetic nanoparticles produced by pulsed laser ablation of thin cobalt films in water, *Bull. Russ. Acad. Sci.: Phys.* 88 (4) (2024) 540–548, <https://doi.org/10.1134/S1062873823706281>.
- [28] L. Russo, F. Colangelo, R. Cioffi, I. Rea, L. De Stefano, A mechanochemical approach to porous silicon nanoparticles fabrication, *Materials (Basel)* 4 (6) (2011) 1023–1033, <https://doi.org/10.3390/ma4061023>.
- [29] V. Yu. Nesterov, O.I. Sokolovskaya, L.A. Golovan, D.V. Shuleiko, A.V. Kolchin, D.E. Presnov, P.K. Kashkarov, A.V. Khilov, D.A. Kurakina, M. Yu. Kirillin, Laser fragmentation of silicon microparticles in liquids for solution of biophotonics problems, *Quantum Elec (Woodbury)* 52 (2) (2022) 160, <https://doi.org/10.1070/QEL17984>.
- [30] L. Zhang, Y. Liu, B. Key, S.E. Trask, Z. Yang, W. Lu, Silicon nanoparticles: stability in aqueous slurries and the optimization of the oxide layer thickness for optimal electrochemical performance, *ACS Appl. Mater. Interfaces* 9 (38) (2017) 32727–32736, <https://doi.org/10.1021/acsami.7b09149>.
- [31] T. Savchuk, I. Gavrilin, A. Savitskiy, A. Dronov, D. Dronova, S. Pereverzeva, A. Tarhanov, T. Maniecki, S. Gavrilov, E. Konstantinova, Effect of thermal treatment of symmetric TiO₂ nanotube arrays in argon on photocatalytic CO₂ conversion, *Symmetry (Basel)* 14 (12) (2022) 2678, <https://doi.org/10.3390/sym14122678>.
- [32] A.S. Steparuk, R.A. Irgashev, G.L. Rusinov, E.V. Krivogina, P.I. Lazarenko, S.A. Kozyukhin, Synthesis and photovoltaic properties of new thieno [3, 2-b] indole-based dyes, *Russ. Chem. Bull.* 68 (2019) 1208–1212, <https://doi.org/10.1007/s11172-019-2542-z>.
- [33] A.S. Steparuk, R.A. Irgashev, E.F. Zhilina, V.V. Emets, V.A. Grinberg, E.V. Krivogina, E.V. Belova, P.I. Lazarenko, G.L. Rusinov, S.A. Kozyukhin, Performance evaluation of dye-sensitized solar cells (DSSCs) based on metal-free thieno [3, 2-b] indole dyes, *J. Mater. Sci. Mater. Electron.* 33 (9) (2022) 6307–6317, <https://doi.org/10.1007/s10854-022-07805-w>.
- [34] E.A. Ponomarev, L.M. Peter, A generalized theory of intensity modulated photocurrent spectroscopy (IMPS), *J. Electroanal. Chem.* 396 (1995) 219–226, [https://doi.org/10.1016/0022-0728\(95\)04115-5](https://doi.org/10.1016/0022-0728(95)04115-5).
- [35] A.C. Fisher, L.M. Peter, E.A. Ponomarev, A.B. Walker, K.G.U. Wijayantha, Intensity dependence of the back reaction and transport of electrons in dye-sensitized nanocrystalline TiO₂ solar cells, *J. Phys. Chem. B* 104 (2000) 949–958, <https://doi.org/10.1021/jp993220b>.
- [36] W. Su, J. Zhang, Z. Feng, T. Chen, P. Ying, C. Li, Surface phases of TiO₂ nanoparticles studied by UV raman spectroscopy and FT-IR spectroscopy, *J. Phys. Chem. C* 112 (20) (2008) 7710–7716, <https://doi.org/10.1021/jp7118422>.
- [37] H.C. Choi, Y.M. Jung, S.B. Kim, Size effects in the Raman spectra of TiO₂ nanoparticles, *Vib. Spectrosc.* 37 (1) (2005) 33–38, <https://doi.org/10.1016/j.vibspec.2004.05.006>.
- [38] S. Nomoev, P.M. Adam, S. Bardakhanov, I. Vasilevskii, A. Movsesyan, E. Khartaeva, A visible light scattering study of silicon nanoparticles created in various ways, in: *AIP Conference Proceedings*, 2288, AIP Publishing, 2020, <https://doi.org/10.1063/5.0028254>.